Revista de la Sociedad Geológica de España 36 (1)

ISSN (versión impresa): 0214-2708
ISSN (Internet): 2255-1379
https://doi.org/10.55407/rsge.96703

MAPPING HYDROTHERMAL ALTERATIONS AND LINEAMENTS ASSOCIATED WITH EPITHERMAL AND MASSIVE SULPHIDES DEPOSITS OF TIFRAOUINE (NORTHWEST ALGERIAN COAST): USE OF LANDSAT 8 OLI DATA AND REMOTE SENSING

Cartografía de las alteraciones hidrotermales y de los lineamientos asociados a los depósitos de sulfuros epitermales y masivos de Tifraouine (costa noroeste de Argelia): Utilización de datos Landsat 8 OLI y teledetección

Bouchera Labdaoui[1], Hanafi Benali[2], Amina Boughacha[1] and Khadidja Moussaoui[2]

[1] *Department of Geophysics, Faculty of Earth Sciences, Geography and Territorial Planning, Houari Boumediene University of Sciences and Technology, USTHB, BP 32 Al Alia, 16111, Algiers.*
l_bouchrati@yahoo.fr, am.boughacha@yahoo.fr
[2] *Department of Geology, Laboratory of Metallogeny and Magmatism, Faculty of Earth Sciences, Geography and Territorial Planning, Houari Boumediene University of Sciences and Technology, USTHB, BP 32 Al Alia, 16111, Algiers.*
hbenali@yahoo.fr, moussaouikhadidja@yahoo.fr

Abstract: *Within the context of studying mineralizations related to the Miocene volcanic rocks from the northern part of Algeria, Landsat 8 OLI data and remote sensing techniques are carried out to characterize and map hydrothermal alteration outcrops in the Miocene volcanic rocks of Tifraouine on the northwestern Algerian coast, where several indications of mineralization are known. Short-wave infrared (SWIR) bands allowed for the identification of clay alterations, while the visible and near-infrared bands help in the detection of iron alterations. Red-green-blue color combination images of 6/7, 4/2 and 5/6 ratios were produced. Principal component analysis (PCA) was computed to characterise altered zones and extract lineaments. Matched filtering technique (MF) allows direct detection after applying minimum noise fraction (MNF) transformation and pixel purity index to the spectra in order to obtain a distribution map of the target mineral species in studied area. The remote sensing results combined with the structural geological data determine a relationship between mineralization and structural features and show that hydrothermal alterations are clearly controlled by tectonic. They are highly concentrated in the calderas zone and extend towards the Bouzedjar area which allowed checking the map performed according to the field studies. This will contribute to preliminary studies related to mineral exploration and enhance the mining potential of Tifraouine. The acquisition of supplementary data would allow us to extend this study in coming works.*

Keywords: *volcanism, alteration, Tifraouine, fractures, detection*

Resumen: *En el contexto del estudio de las mineralizaciones relacionadas con las rocas volcánicas del Mioceno de la parte norte de Argelia, los datos del Landsat 8 OLI y las técnicas de teledetección se han utilizado para caracterizar y cartografiar los afloramientos de alteración hidrotermal en las rocas volcánicas del Mioceno de Tifraouine, en la costa noroeste de Argelia, donde se conocen varios indicios de mineralización. Las bandas del infrarrojo de onda corta (SWIR) permitieron identificar las alteraciones de la*

arcilla, mientras que las bandas del visible e infrarrojo cercano ayudaron a detectar las alteraciones del hierro. Se obtuvieron imágenes de combinación de colores rojo-verde-azul de proporciones 6/7, 4/2 y 5/6. Se realizó un análisis de componentes principales (PCA) para caracterizar las zonas alteradas y extraer los lineamientos. La técnica de filtrado emparejado (MF) permite la detección directa después de aplicar la transformación de fracción de ruido mínima (MNF) y el índice de pureza de píxeles a los espectros, para obtener un mapa de distribución de las especies minerales objetivo en el área estudiada. Los resultados obtenidos por teledetección muestran que las alteraciones hidrotermales están claramente controladas por rasgos tectónicos. Están muy concentradas en la zona de las calderas y se extienden hacia la zona de Bouzedjar, lo que permitió comprobar el mapa realizado según los estudios de campo. Esto contribuirá a los estudios preliminares relacionados con la exploración minera y mejorará el potencial minero de Tifraouine. La adquisición de datos complementarios permitirá ampliar este estudio en los próximos trabajos.

Palabras clave: *vulcanismo, alteración, Tifraouine, fracturas, detección*

Labdaoui, B., Benali, H., Boughacha, A., Moussaoui, K., 2023. Mapping hydrothermal alterations and lineaments associated with epithermal and massive sulphides deposits of Tifraouine (northwest Algerian coast): Use of Landsat 8 OLI data and remote sensing. *Revista de la Sociedad Geológica de España*, 36 (1): 3-15.

Introduction

Information about the Earth's surface can be collected by satellite remote sensing, without any direct physical contact. This process consists in collecting emitted electromagnetic energy, which is then analysed and interpreted. Worldwide, several studies have been conducted in the identification of minerals forming zones using remote sensing (Ninomiya, 2003; Azizi *et al.*, 2007; Mia and Fujimitsu, 2012; Rockwell, 2013; Abdelnasser *et al*., 2018; Cardoso-Fernandes, 2019; Adiria *et al*., 2020; Peleli *et al*., 2021; Yousefi, 2021). The supergene phase and iron oxides occurred on the surface are indicators of mineralization (Torres-Vera and Prol-Ledesma, 2003; Eisele *et al*., 2012; Pour *et al*., 2013) therefore, remote sensing technologies are suitable tools for identifying hydrothermal alterations, especially in the early stages of investigation, in the analysis of the relationship between mineralizations and structural elements as demonstrated in Sar cheshmeh copper mining district in Iran (Pour and Hashim, 2015), in Tirka Area, Toroud, NE Iran (Mina *et al*., 2019) and in the Guelma basin (Northeastern Algeria) (Nait Amara *et al*., 2019). The Landsat 8 satellite was launched on February 11, 2013. It was developed by NASA in collaboration with the USGS (United States Geological Survey). The thermal instrument (TIRS) carries two additional thermal infrared bands, band 10 and band 11. The Operational Land Imager of Landsat 8 data (OLI) is able to identify hydrothermal alterations due to their absorption and reflectance features that occur in this range (Ali and Pour, 2014; Amin Beiranvandet *et al*., 2014; Mwaniki *et al*., 2015; Wang *et al*., 2017). In northwest Algeria, more particularly in Tifraouine, mineralizations related to hydrothermal alteration are hosted in Miocene volcanic rocks. The volcanic massif of Tifaraouine belongs to the volcanic group of the Sahel of Oran. The region has been the subject of geological and geophysical studies revealing the existence of several mineralization indexes. The region's mining potential started in colonial times (Glaçon, 1967). Several small deposits have been discovered during prospecting campaigns, the most important is the Oued Chadia magnetite deposit, discovered and prospected in 1856 until 1859.

The purpose of this article is to present a distribution map of altered rocks by the use of satellite remote sensed data and to compare it with that obtained by field studies. In this study, different approaches of detection methods were used with various image processing and enhancement techniques applied to Landsat 8 data (OLI). These data have been chosen in this study due to its availability and resolution. More than that, The OLI and TIRS sensors of Landsat 8 data improve the radiometric performance of the signal-to-noise ratio and allow data quantification with better land coverage (Pour and Hashim, 2015). Indeed, several studies around the world in geosciences proved that remotely sensed multispectral data is a powerful tool for mineral exploration, identification of hydrothermal alteration zones and determination of structural features allowing the acquisition of valid results (Ducart *et al*., 2016; Hu *et al*., 2018; Ibrahima *et al*., 2018; Nait Amara *et al*., 2019; Adiria *et al*., 2020; Peleli *et al*., 2021). Thus, the main objectives of this work are to map hydrothermal alterations in the Miocene volcanic rocks of Tifraouine and extracting lineaments to solve the following problems: how does hydrothermal alterations occur in Tifraouine? What is the relationship between structural elements and hydrothermal alterations? Are there similarities between the results of field studies and those of remote sensing?

Geology of Tifraouine

The Miocene volcanic rocks of Tifraouine are located on the northwest Algerian coast, forty kilometers southwest of

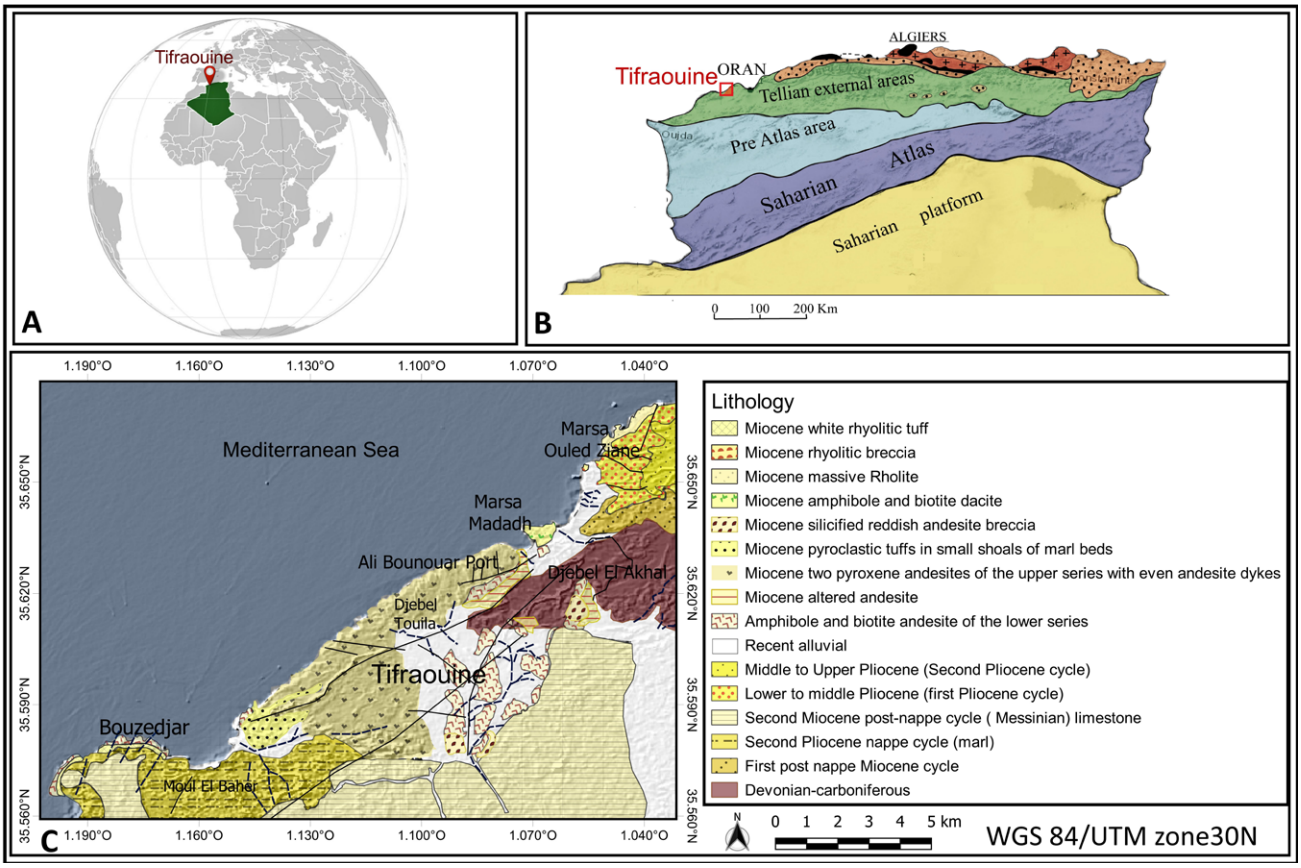

Fig. 1.- A) Location of the study area. B) Situation of Tifraouine in relation to the major morphological complexes of northern Algeria (Himri, 2008).C) simplified geological map of Tifraouine (Megartsi, 1985).

Oran, thirty kilometers north of EL Amria city (Ain Temouchent) and ten kilometers northwest of the Sebkha of Oran, between Bouzedjar Port to the southwest and the Ali Bounouar Port to the northeast (Fig. 1). This region is characterized by a warm temperate climate with an annual rainfall of about 378 mm and sparse Mediterranean vegetation. It is marked by moderate land elevations, with altitudes of no more than 300 metres (Belmouhoub, 1995; Benali, 2007). Thanks to geological studies, several gold and copper targets have been detected in Tifraouine with concentrations of elements such as copper, gold, nickel, vanadium, lead and zinc (Mouffok, 1999; Souahlia, 2001; Belmouhoub, 2004). In the context of the polymetallic mineral research related to volcanic and volcanosedimentary rock of northwestern Algeria, geologists of the Algerian National Office for Geological and Mining Research (ORGM) suggest the existence of a Kuroko-type deposit in Tifraouine (Belmouhoub, 2004). To better characterize mineralization and hydrothermal alterations, three boreholes performed by the ORGM were studied by Belmouhoub (2004) and Benali (2007). In 1996, mapping the distribution of hydrothermal alterations in Tifraouine was realized by the ORGM through field studies, that shows the degree of hydrothermal alteration in the caldera of Tifraouine (Fig. 2).

The Miocene volcanic rocks of Tifraouine belong to the volcanic complex along the coast of Oran in western Algeria, situated in the western sector of the Tellian external area that forms the southern segment of the alpine chain

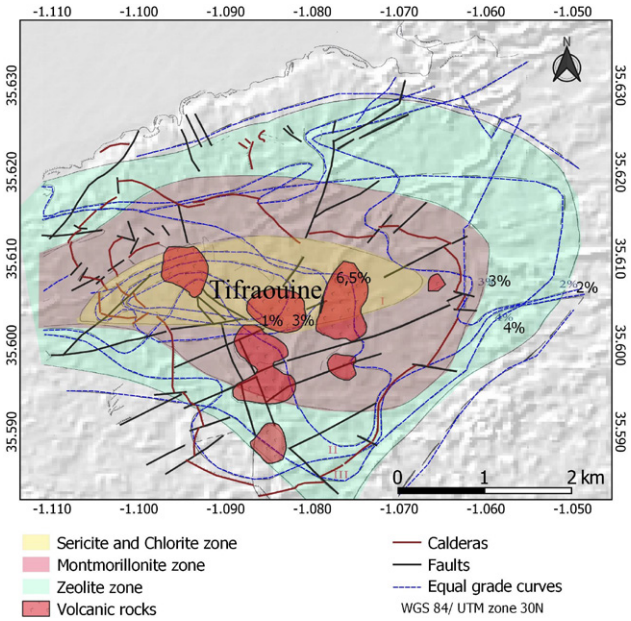

Fig. 2.- Hydrothermal alteration map of Tifraouine developed according to field studies performed by Belmouhoub (2004).

(Fenet, 1975; Guardia, 1975; Megartsi, 1985; Ciszak, 1993; Pique *et al*., 1998) (Fig. 1). It consists of folded Mesozoic formations below Cenozoic rocks and intense Miocene volcanic activity that began approximately 9.7 million years ago (lower Tortonian) and ended 7.9 million years ago (late Tortonian) (Megartsi, 1985; Benali, 2007).

The common rocks are pyroxene and amphibole andesites, tuffs and hydrothermally altered rhyolitic dacites, giving rise to copper, gold, lead and zinc mineralization.

Two volcanic stages have been identified in Tifraouine. The first stage began with an emission of volcanic ash and deposited a tuff layer a few metres thick, followed by an emission of lava and pyroclastic flows that formed pyroclastic breccias, while the second stage is characterized by an early and abundant emission of ash that created a volcanosedimentary formation with lava and coarse pyroclastic material and a formation of the Tifraouine calderas as the volcano collapsed, allowing the intrusion of andesitic and dacitic lava. All lavas in Tifraouine have petrographic characteristics of the calc-alkaline series (Benali, 2007).

Hydrothermal alterations are described by rocks exposed to different physical-chemical conditions at which they were originally formed reflecting new minerals by the actions of hydrothermal fluids (Woldai *et al*., 2010). In order to verify the presence of argillic, propylitic, sericitic and iron alterations on the surface around the caldera of Tifraouine, the observed alteration types on several levels are propylitization, expressed by calcite, epidote and chlorite; argilitization pronounced by kaolinite and illite; sericitization characterized by muscovite and oxidation described by iron oxides such as jarosite, hematite and goethite.

Following its formation, the Tifraouine volcano was affected by a series of tectonic accidents giving it a circular caldera structure with a diameter of 2.5 to 3 km, enclosing the Chadia wadi index. This caldera is itself contained within another concentric circular structure of 9 km in diameter that includes the Djebel Touila deposit (Belmouhoub, 1995). At the regional scale, Tifraouine is situated within the limits of littoral horst, characterized by secondary uplifts (in particular, Madakh uplift) and faults of various directions (Guardia, 1975). El Akehal Mountain is the tectonic framework of Tifraouine, located between the main faults of the region, where tectonic directions are NE-SW. In the Mesozoic bedrock of Tifraouine, two fault systems are nearly parallel to the main faults and major structural alignments of the Oran coastal area. The first series of NE-SW direction is at the origin of the general orientation of the anticline structures resumed in the form of horst. The N60ºE-N70ºE trending fault of El Akhal Mountain directed N60°- N70° is related to this system of faults. The second series is synchronous and perpendicular to the first. These are transversal faults in which the main outflows occur and set up two mineralized deposits (Touila Mountain and Wadi Chadia) (Fig. 3).

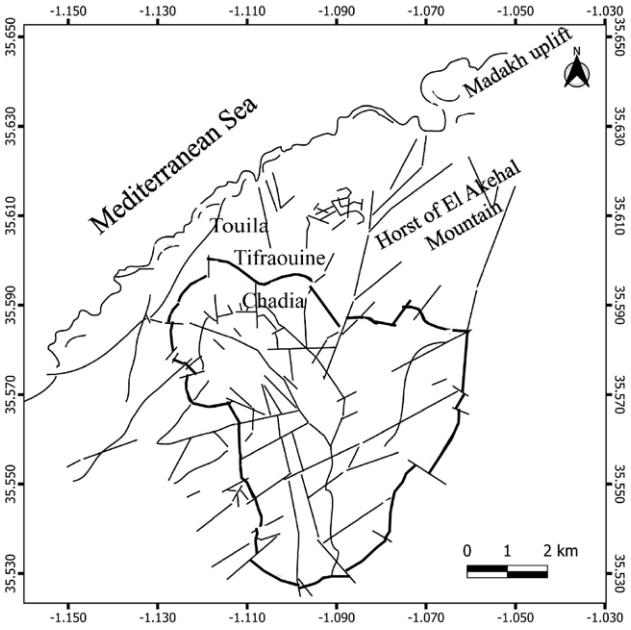

Fig. 3.- Structural map of Tifraouine (Belmouhoub, 1995).

Remote sensing and data analysis: Landsat 8 imagery

A cloud-free level 1T (terrain-corrected) Landsat 8/OLI/TIRS sensor imagery (path/row 198/35) of the Tifraouine area was downloaded from the (USGS) (http://earthexplorer.usgs.gov) in the TIFF format and projected to the WGS 84 datum in the Universal Transverse Mercator zone 30 North. The image used in this study was acquired by the satellite on 18 June 2013. For geological purposes, data collected in the visible and near-infrared (VNIR) and short-wave infrared (SWIR) bands are of principal interest (Frutuoso *et al*., 2021; Zanter, 2016). Seven of these nine bands are consistent with the Thematic Mapper (TM) and Enhanced Thematic Mapper Plus (ETM+).

Geological mapping involved using typical absorption characteristics of chemical elements that compose minerals through spectral signatures in the spectral range (Pour and Hashim, 2015), that allows their detection and recognition. For example, montmorillonite shows absorptions around ~1413 nm and ~1911 nm, with the Al-OH features at ~2206 nm (Pontual *et al*., 2008; Clark *et al*., 1990), lower than ~1911 nm, and a slight inflection around ~1467 nm (Cardoso-Fernandes *et al*., 2022). Three bands can be effective in the mineral determination process. Band seven is the absorption band caused by clay mica, hydrous mineral, sulfates and some oxides. Band 6 refers to iron-rich or hematite rocks and is used in soil and rock discrimination. Band 4 is good in delineating soil cover and is used in the discrimination of soil from vegetation (Nait Amara *et al*., 2019).

Data preprocessing and methodology

The Landsat 8/OLI data of the study area were pre-processed and calibrated with ENVI software, by converting Landsat 8 calibrated digital numbers (DNs) to physical units; values of surface reflectance (SR) were obtained by the application of Fast Line of Sight Atmospheric Analysis of Hypercubes (FLAASH) algorithm of ENVI software (ENVI Tutorial, 2013). Hydrothermal alterations (clay, propylitic, iron and sericitisation) can be enhanced by using color composites (true color combination and false color combination images), band rationing (Sabin's ratio 5/6, 4/2 and 6/7) and spectral target detection tool by direct comparison with spectra of minerals in the spectral library. After these corrections, the resulting spectra can be compared directly with those of the spectral library (Scheidt, 2008).

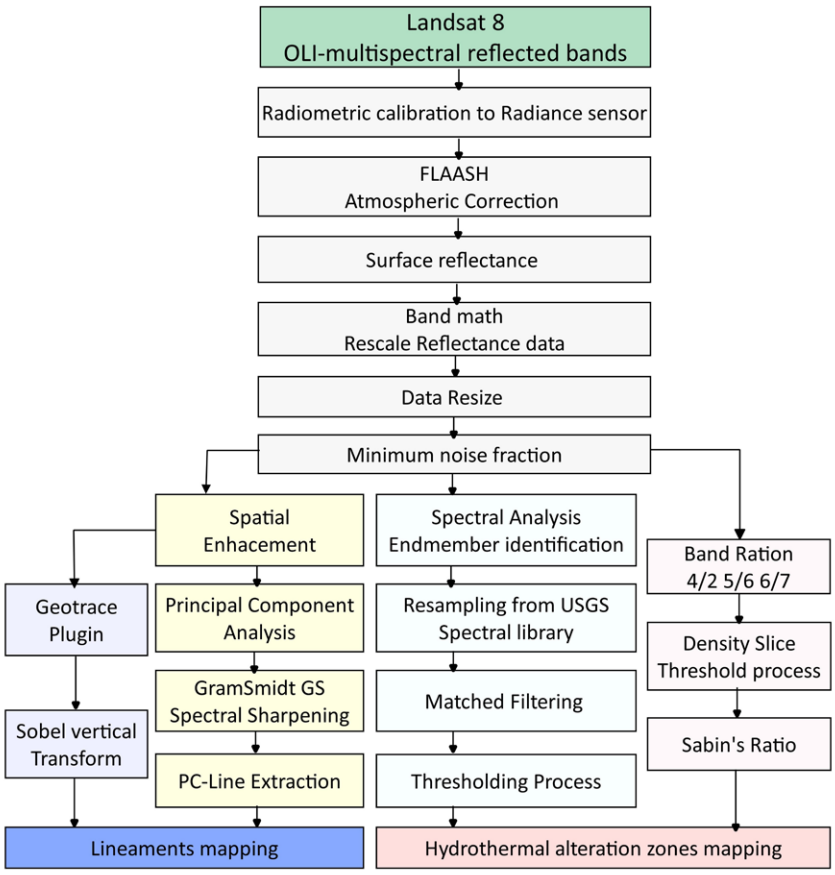

Fig. 4.- Workflow of Landsat 8 OLI data.

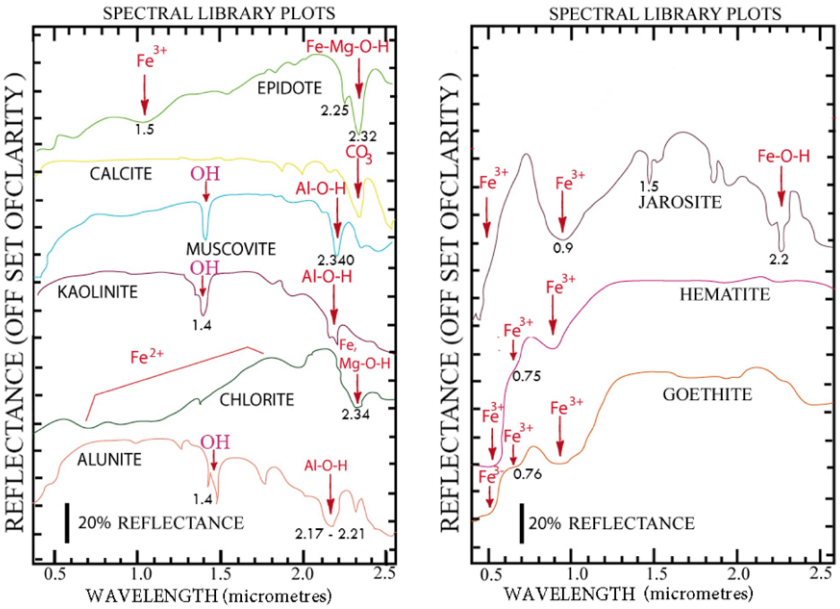

Fig. 5.- Laboratory spectra of the detected minerals used in the current study (Clark *et al*., 1993).

The additional data used are geological and structural maps with an existing hydrothermal alteration map of Tifraouine Belmouhoub (2004) and Benali (2007). Three software packages that would process all steps analysis were used, in particular those of ENVI, QGIS and Geomatica. To extract hydrothermal alteration-related spectral and spatial data, the Minimum Noise Fraction (MNF) transformation was used to define the specific size of the data (Green *et al*., 1988). Band combination, band ratio, principal component analysis (PCA) and matched filtering (MF) were applied as image enhancement techniques. The preprocessing and processing schema used for Landsat 8 OLI data is summarized in a flow-chart (Fig. 4). A reflectance spectrum allows the discrimination of minerals as the optical spectrum of a mineral is directly related to its chemistry and crystallography (Turner *et al*., 2014). In the studied area, the clay alteration is represented by kaolinite with doublet absorption features at 2.165 and 2.200 µm. Illite has water absorption at 1.9 µm, 1.9 µm, Al-OH absorption characteristics at 2.20, ~2.34 and ~2.44 µm. Alunite has absorption features at ~2.17, 2.21 µm derived from Al-OH, and ~2.40 µm derived from S-O (Pontual *et al*., 2008; Fig. 5). Muscovite is a typical mineral in phyllic alteration, with distinct Al-OH absorption features at 2.20 µm and a less intense absorption features at 2.35µm. Chlorite, calcite and epidote are typical minerals of propylitic alteration, with absorption features of chlorite at 2.254 µm (Fe-OH) and (Mg-OH) absorption at 2.347µm (Fig. 5). Calcite has an absorption of C-O at ~2.345 µm which persist in mixtures (Fig. 5). Epidote has absorption features at ~1.545 µm that distinguishes it from chlorite and helps to identify epidote in mixtures (Fig. 5). Iron oxides such as jarosite having Fe–O–H absorption features at 0.94 and 2.27 µm (Hunt, 1977). Hematite is characterized by a peak at ~750 nm which gives it its distinctive red colour, weaker (Fe^{3+}) iron absorption at ~0.66 and 0.890 µm, derived from ferric iron. Goethite is characterized by a peak at ~0.76 µm which gives the distinctive red, orange colour to goethite, diagnostic ferric Fe^{3+} iron absorptions at ~0.66 nm and ~0.91 - 0.94 µm (Pontual *et al*., 2008).

Mapping hydrothermal alteration

Color composites

Tifraouine is characterized by average vegetation that is concentrated in the coastal zone and extends with the

drainage system. For the identification of hydrothermal alteration minerals associated with the volcanic rocks of Tifraouine, green, red, blue (RGB) colour combination images and band ratios were created with the Landsat 8 OLI data spectral bands. The combination RGB 4, 3 and 2 is a representation of true color; the land cover nature is represented by the color combined images 5, 6 and 7.

Band ratio

Ratio is calculated by dividing the numerical value of a selected band by that of the other one which produces images of the relative band intensities; it is a technique known for highlighting certain features and materials that cannot be seen in raw bands (Inzana, 2003). They have been used for many years in the field of remote sensing to display spectral variations (Goetz *et al*., 1983), and also for reducing the topographic effect (Segal, 1983). Unique information may be extracted from band ratios, which would otherwise not be available from any single band. For this reason, these ratios have been successfully used to map altered areas (Jensen, 1996). In the current study, combination of RGB images called Sabin's ratio 5/6, 4/2 and 6/7 have been used to highlight iron oxides, clays and ferrous minerals (Sabins, 1999). The ratio 4/2 is useful for mapping iron oxides (hematite, goethite, jarosite, etc.) because they have absorption in the low blue region (band 2), while they have a high reflectance in the near red region (band 4). As they show high reflectance characteristics in band 5 and strong absorption features in band 6, ferrous minerals such as olivine, pyroxenes and amphiboles are mapped by the ratio 5/6 (Gupta, 2003, 2017). The ratio 6/7 was used for its capability to map kaolinite, montmorillonite (clay minerals), micas, alunite and talc–carbonates, etc. (Rowan *et al*., 1977; Goetz and Rowan, 1981; Frutuoso *et al*., 2021); all these minerals show high reflectance in band 6 and lower reflectance in band 7 of Landsat 8 OLI data. It enhances also vegetation (Agar and Coulter, 2007; Ducart *et al*., 2016).

Principal components analysis

PCA is widely applied to multispectral and hyperspectral remotely sensed data. It reduces data dimensionality (e.g., number of bands) and condenses the information in intercorrelated variables into a few variables (Jensen, 2005; Buenemann, 2011; Pour and Hashim, 2015). Usually, the first principal components PC1, PC2, PC3 containing the majority of information were selected for RGB display. This is the combination selected for interpretation.

Matched filtering

Supervised classifiers are usually applied to hyperspectral data but can also be applied to multispectral data. Therefore, maps of the mineral abundance can be produced. By this approach, data were analyzed to determine unique spectral end-members and their spatial distribution by producing detailed maps. This process requires several steps: spectral compression, noise removal by a linear transformation, MNF (Green *et al*., 1988) that consists of the following separate principal components analysis. The first rotation uses the principal components of the noise covariance matrix to decorrelate and rescale the noise in the data. The second rotation uses the principal components derived from the original image data after they have been noise whitened by the first rotation and rescaled by the noise standard deviation (Boardman *et al*., 1994). The MF method is described by Harsany and Chang (1994) and Boardman *et al*. (1998). This technique does not require knowledge of all the end-members within an image scene and can be used in the identification of single feature types. This method aims to identify individual minerals directly by target detection. To apply the MF algorithm, reference spectra must be selected from the spectral library or image collections and compared directly with the extracted spectra. It was applied to VNIR and SWIR bands of Landsat 8 OLI/TIRS data to map clays, sulfates, sericitic, propylitic mineral groups and Fe-oxides/hydroxides for each hydrothermal alteration mineral shown by automated identification and comparison with the spectral library. This is relatively insensitive to the magnitude of reflectance; therefore, the classification result is not affected by bidirectional reflectance effects or low to moderate shadowing. MF is able to quantitatively estimate the probability of a mineral occurrence and has been shown to result in excellent detectability and selectivity for spectrally distinct minerals (Boardman, 1998).

The MF algorithm equation is expressed as follows: $Fx = t - mTs - 1(x - m)$, where x represents the sampled vector, T concerns the targeted vector, m is the background mean and s the background covariance (Schott, 2007). This algorithm is the only one that could provide in such conditions semi-quantitative information (Van Der Meer and Steven, 2001; Santos *et al*., 2022). For the production of the distribution maps of the alteration minerals, the threshold processes are applied to the MF score (Fig. 6).

Structural elements and lineaments in Tifraouine

Several studies have revealed an important correlation between mineral deposits and lineaments, so the interpretation of lineaments and fractures is important in targeting ore deposits (Nait Amara, 2019; Cardoso-Fernandes, 2022). The tonal differences within the surface are reflected as direct lines on the satellite images that can be interpreted as visible lineaments (Zamyad *et al*., 2019). The dominant direction of lineaments in Tifraouine is NW-SE. It is related to the general orientation of the anticlinal structures resulting from the movements responsible for the formation of the coastal horst on a regional scale. To characterise and map lineaments in Tifraouine, it is necessary to extract the principal components (PC) and then choose the first principal component as it contains the most data information. Automatic lineament extraction from the PC1 Pansharpened band is performed with a PC-Line extractor in Geomatica software. The Geotrace plugin in QGIS provides and eases the identification of faults and fractures by using filters on Landsat 8 OLI data multispectral images, notably Sobel vertical transform. After this processing, the

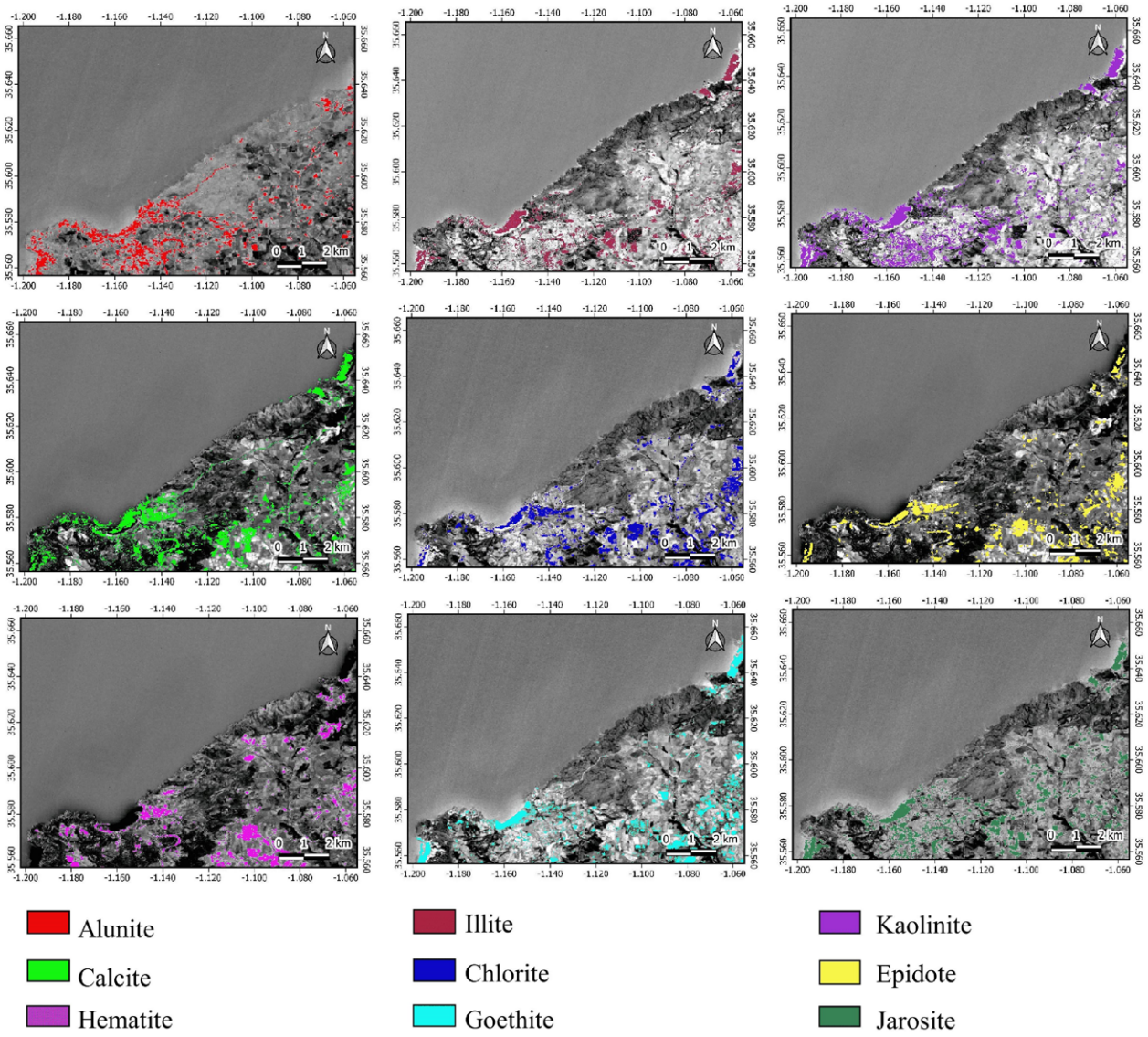

Fig. 6.- Mineral maps showing the results of MF method using Landsat 8 OLI data.

resulting lineaments were manipulated by Geographic Information System (GIS) software where the data were digitised, grouped and then mapped and statistically analysed to create rose diagrams for interpretation.

Results, discussion and validation

The intersection of lineament density with hydrothermal alteration zones is an indicator of mineralization (Rameshchandra, 2014). Results obtained from Landsat 8 satellite image processing techniques were compared to existing geological data including information about alteration, tectonic and lineaments of Tifraouine using GIS software. The combination RGB in Fig. 7A is a representation of true color and in Fig. 7B it shows rocks and soils in white and bluish pixels. The red and brownish area corresponds to natural and plantation vegetation.

Band rationing was used to create the False Colour Composite (FCC) image of 6/7, 6/5, 4/2 called Sabin's ratio. We obtain clays minerals (micas and talc–carbonate) in the bluish areas with vegetation in bright cyan pixels, iron oxides (hematite, goethite, and jarosite) in reddish areas and ferrous minerals in greenish areas (Fig. 8). The 6/7 ratio is commonly used to detect clays and vegetation (Da Cunha Frutuoso, 2015) because the spectra show high vegetation reflectance in the SWIR1 and low in the SWIR2 (Nait Amara *et al*., 2019). Therefore, it is expected that vegetation covering mineral deposits will have different reflectance curves than those growing in non-mineralized areas. The color patterns in the individual density-sliced images are different (Sabins, 1999). The use of the density slice option for each ratio in the ENVI by introducing threshold values, helps to highlight hydrothermal alterations (Fig. 9). The high-brightened areas show the potential target minerals (Cudahy *et al*., 2008; Rockwell, 2013; Eldosouky *et al*., 2017). Stages of mapping alterations by ratio bands are shown in Fig 10 as a flow chart and results are shown in Fig. 11. The PCA results in Fig. 12 show the ferrous minerals in light green and the iron oxides in greenish yellow pixels.

As shown in Fig. 13, mapped and collected lineaments are mainly distributed along the NE-SW direction which is

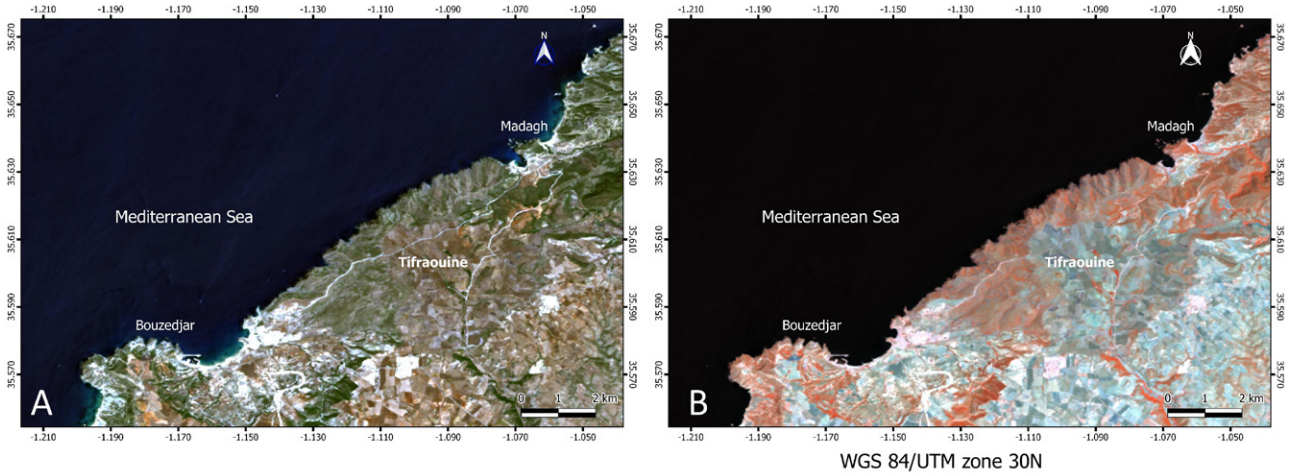

Fig. 7.- Composite color maps. A) True color image RGB combination of bands 4, 3, and 2. B) RGB combination of bands 5, 6, and 7.

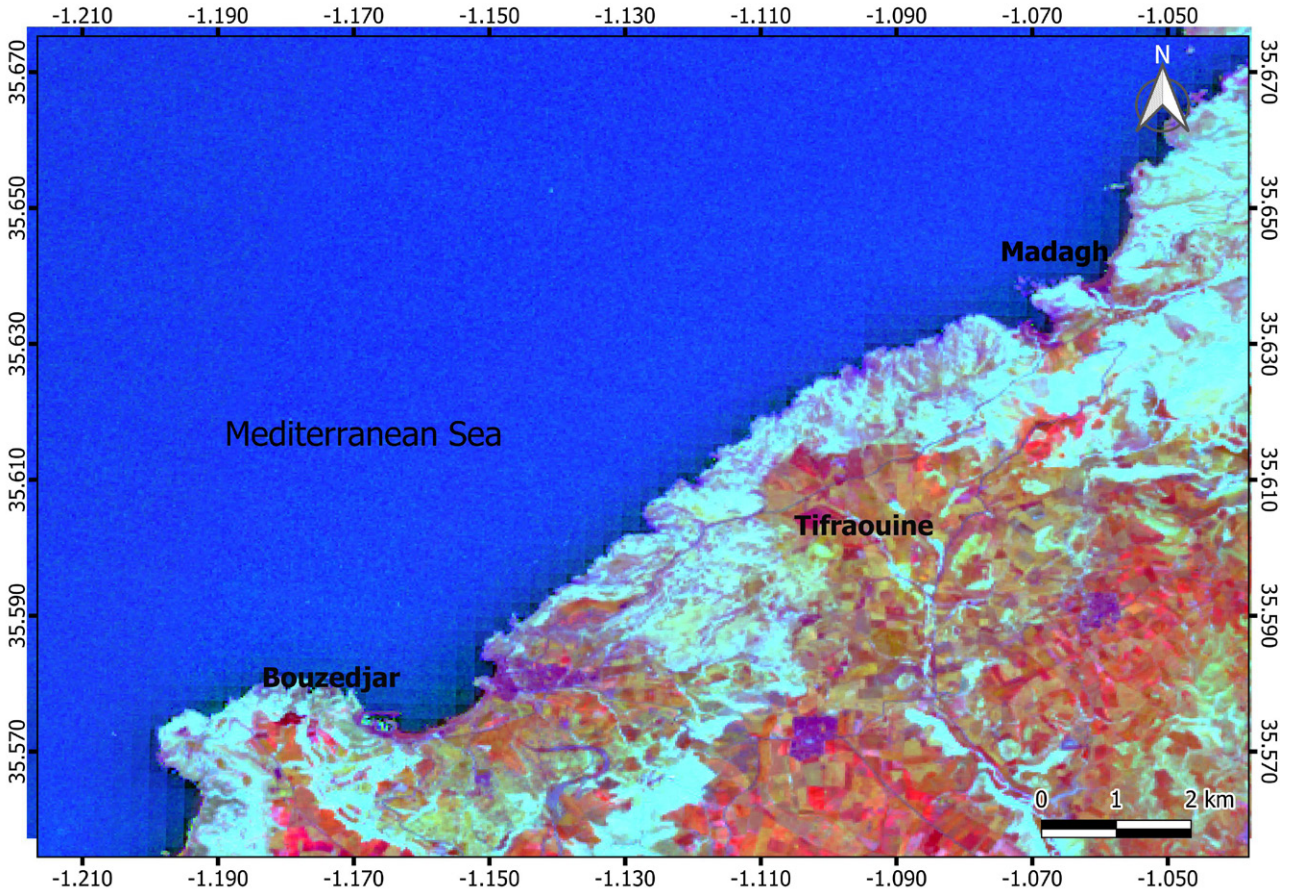

Fig. 8.-Combination of 6/7, 5/6, 4/2 in RGB composition image reveals the alteration areas in bright cyan and bright pink color.

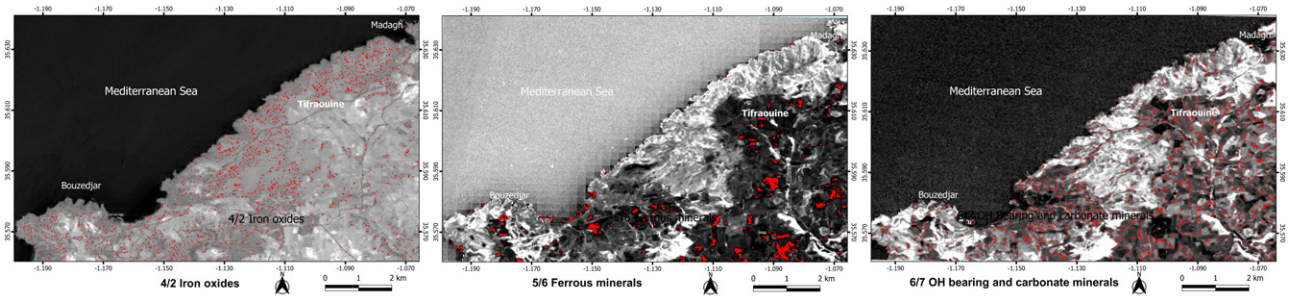

Fig. 9.-Hydrothermal alterations of each ratio using density slicing by introducing threshold values. From left to right: 4/2 iron oxides, 5/6 ferrous minerals, and 6/7 OH bearing and carbonate minerals.

effectively the direction of the major faults of Tifraouine and the most predominant ones corresponding globally to the orientation of the entire region and correspond to what was revealed by the field studies. Through remote sensing, other faults of NW-SE direction have been identified, in addition to some W-E transverse faults, probably those along which the main flows occurred in relation to the mineral deposits of Touila and Chadia. The large caldera of Tifraouine has been identified, including another circular structure representing a second caldera. They are pierced by several fractures that occurred after the formation of the Tifraouine volcano, notably on its NW side. Due to the density of accidents in this part of the caldera, the interaction of hydrothermal fluids along the fractures carrying the mineralizing fluids is important, therefore this zone is probably rich in mineralizations. Results of matched filtering method and band rationing applied to OLI/Landsat 8 data were superimposed on the existing lineaments to create one representative figure of the four types of alteration; this figure shows a spatial distribution of alterations between the two regions Tifraouine and Bouzedjar region (Fig. 14). The comparison of the results obtained by remote sensing and those of the field studies reveals that alterations extend from the Tifraouine calderas to the Bouzedjar area. The clay alteration occurs near the caldera and extends towards the Bouzedjar area through faults and fractures. Sericitic alteration is represented by muscovite and is more extensive. Iron alteration is represented by goethite, haematite and jarosite and shows a broad distribution in the studied areas. Propylitic alteration is the most abundant type of alteration and is observed in more areas (Fig. 14). There is a similarity between the results obtained by the field studies and those we have obtained by remote sensing. The combination of lithological information, structural, and the hydrothermally altered areas defines a new exploration targets (promising zones of mineralization). Thus, the detail obtained in this study allows to extend the study area towards the western side of Bouzedjar to better understand the evolution of these alterations. For more detail and accuracy, the area needs to be further explored with more field studies and taking into account the structural factor that plays a major role in the migration of hydrothermal fluids carrying mineralization.

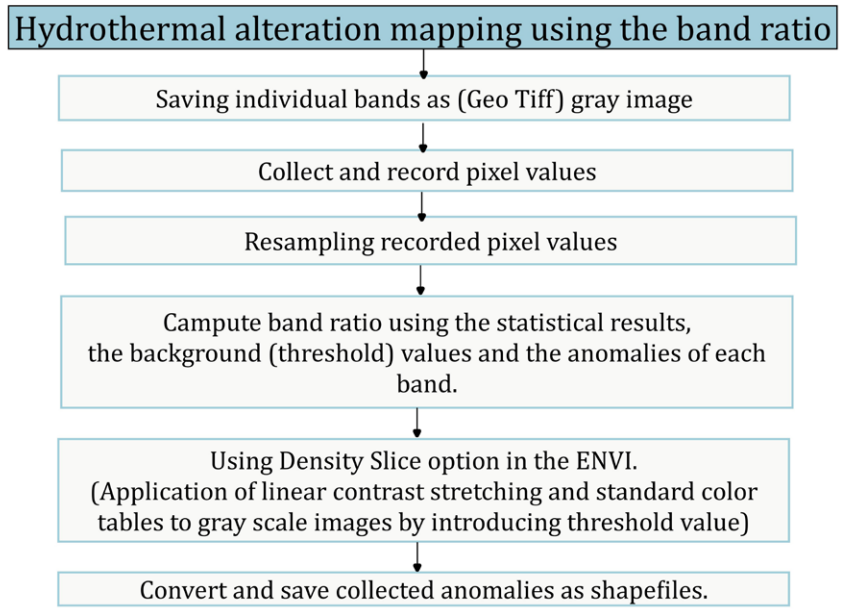

Fig. 10.-Flowchart of hydrothermal alteration mapping steps by band ratios.

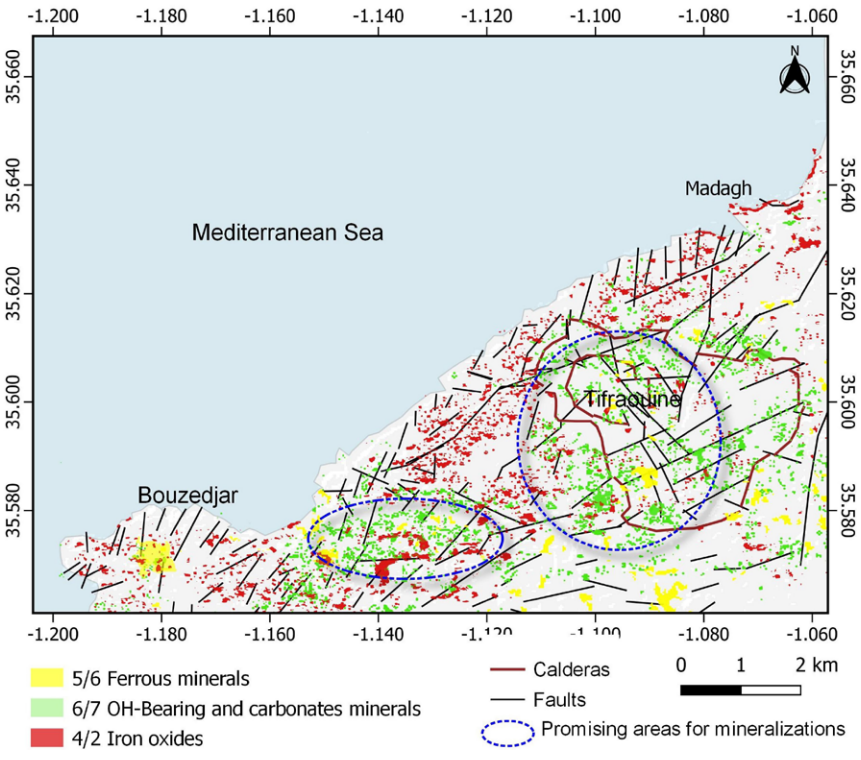

Fig. 11.- Mapping of hydrothermal alteration by ratio bands. Superimposition of the three ratios results.

Conclusion

In this study, we have provided a new distribution map of alteration in Tifraouine for each type of clay, propylitic, iron and sericitic alteration selected to be detected by remote sensing to enhance potential mining exploration areas, especially those related to hydrothermal acti-

vity in Tifraouine and Bouzedjar. The specific band ratio (Sabin's) highlights clay and iron alteration and thus shows that clays are abundant in Tifraouine and Bouzedjar, also concentrated throughout the water flow system, as well as in faults and fractures. All results were pooled and mapped to identify four representative maps for each type of alteration (clay, propylitic, sericite and iron). Direct detection by MF has been applied to SWIR and VNIR bands of Landsat 8 data to verify the results of previous methods, providing clearer and more accurate information on the detection and distribution of alteration minerals, and confirming previous findings that mineralization is concentrated around the caldera of Tifraouine and in the western sector namely Bouzedjar. Maps obtained from processed Landsat 8 OLI satellite images, through the integration of hydrothermal alteration zones in the GIS with previous studies; show that the Tifraouine and Bouzedjar areas have significant mining potential. From the results obtained by various processing and mapping methods, as well as after superimposing the distribution of hydrothermal alterations on the mapped lineaments and the pre-existent volcanic formations, it can be deduced that hydrothermal alterations are controlled by volcanism and the typical structural features in Tifraouine. The processing of Landsat 8 images has allowed the highlighting of hydrothermal alterations and some structural features in Tifraouine, which proves the existence of these hydrothermally altered minerals as previously shown by the field studies. Nevertheless, it is very evident that the use of higher-resolution images will enable better precision and enhancement of the results and this will be the objective of the next studies in this region.

Acknowledgements and funding

Authors would like to express their deepest gratitude to the National Aeronautics and Space Administration for providing free access to satellite data. They are sincerely indebted to their colleagues at the

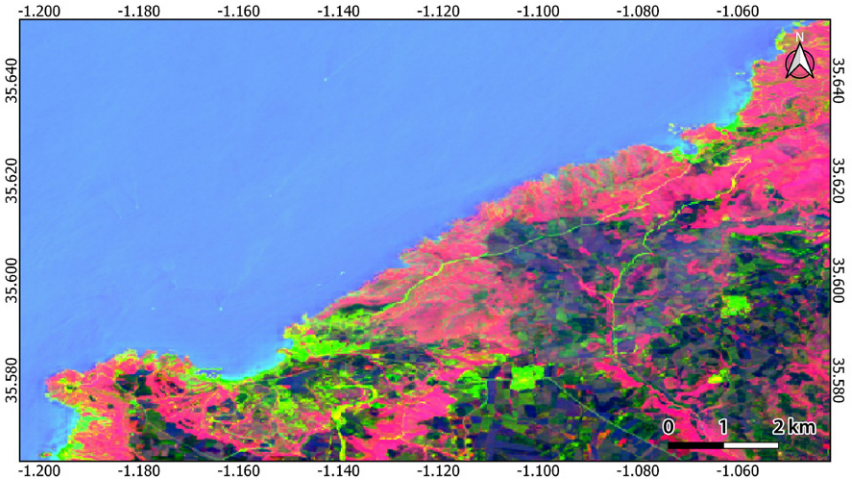

Fig. 12.- RGB color combination of PC1, PC2, and PC3, showing the results of PCA. PC1 in the blue channel, PC2 in the green channel and PC3 in the red channel.

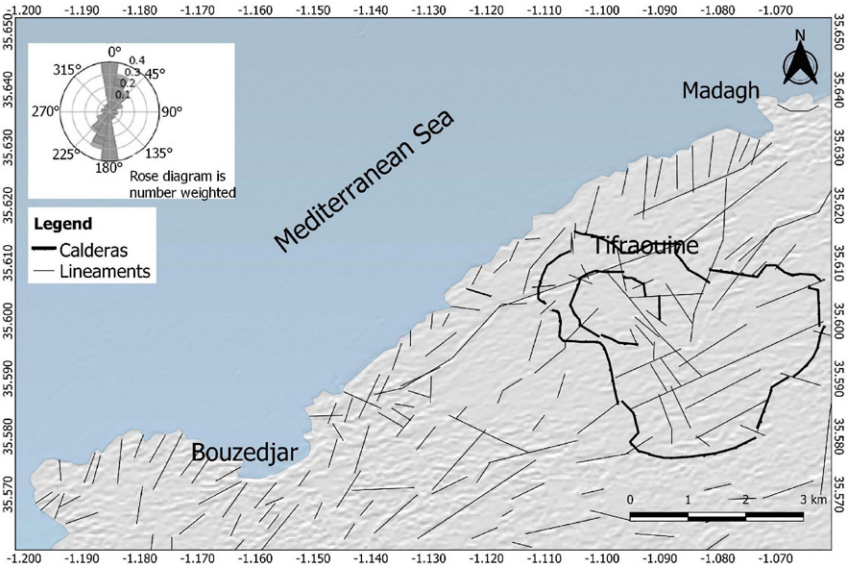

Fig. 13.- Lineament extraction in Tifraouine using the first principal component and PCLine extractor.

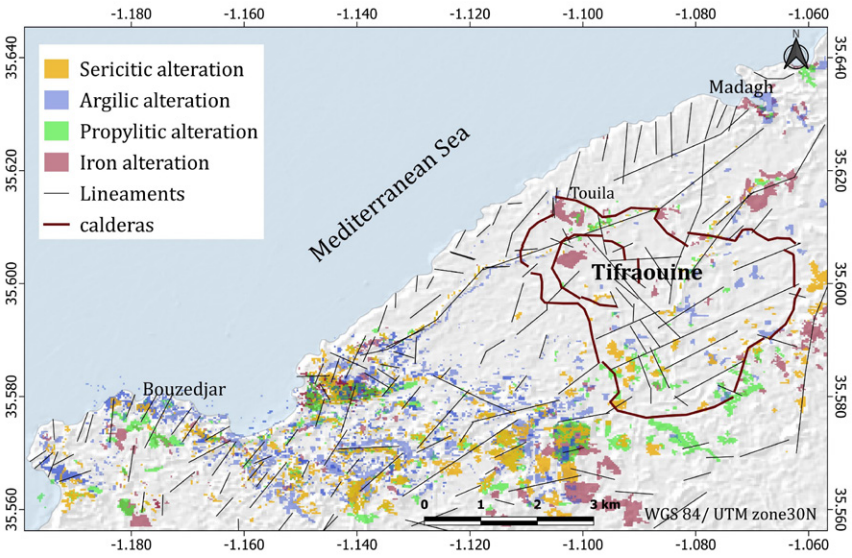

Fig. 14.- Distribution map of hydrothermal alterations in Tifraouine.

"Image Processing and Radiation" Laboratory of the Faculty of Electronics (USTHB) for their contributions and collaboration. The authors would also like to extend their heartfelt appreciation to the Journal Editor for the invaluable corrections, advice, and suggestions, which greatly improved the manuscript. They are also grateful to the anonymous reviewer and Dr. Kamel Amri for their constructive comments that further enhanced the quality of the research. Lastly, the authors would like to indicate that the present research did not receive specific support from public sector agencies, commercial sectors, or non-profit entities.

Author contributions

The individual contribution of each author and elaboration to the work: manuscript preparation, B.L., H.B.; methodology, B.L., H.B., A.B.; data curation, B.L., K.M.; data processing, B.L., K.M.; figures, H.B., K.M., A.B.; research/analysis, B.L., H.B.; manuscript review, H.B., B.L., A.B.; coordination, H.B.; supervision, B.L.

References

Abdelnasser, A., Kumral, M., Zoheir, B., Karaman, M., Weihed, P., 2018. REE geochemical characteristics and satellite-based mapping of hydrothermal alteration in Atud gold deposit. Egypt. Journal of African Earth Sciences, 145: 317-330.

Adiri, Z., Lhissou, R., El Harti, A., Jellouli, A., Chakouri, M., 2020. Recent advances in the use of public domain satellite imagery for mineral exploration: A review of Landsat-8 and Sentinel-2 applications. Ore Geology Reviews, 117: 103332. https://doi.org/10.1016/j.oregeorev.2020.103332

Agar, B., Coulter, D., 2007. Remote sensing for mineral exploration a decade perspective 1997-2007. In: Milkereit B (ed) Proceedings of Exploration 07. Fifth Decennial International Conference on mineral Exploration, 109-136.

Ali, A., Pour, A., 2014. Lithological Mapping and Hydrothermal Alteration Using Landsat 8 Data: A Case Study in Ariab Mining District, Red Sea Hills, Sudan. International Journal of Basic and Applied Sciences, 3, 199-208. https://doi.org/10.14419/ijbas.v3i3.2821

Amin Beiranvand, P., Mazlan, H., 2014. Hydrothermal alteration mapping from Landsat 8 data, SarCheshmeh copper mining district, south-eastern Islamic Republic of Iran. Journal of Taibah University for Science 9 (2015) 155-166. https://doi.org/10.1016/j.jtusci.2014.11.008

Azizi, H., Rsaouli, A.A., Babaei, K., 2007. Using SWIR bands from ASTER for discrimination of hydrothermal altered minerals in the Northwest of Iran (SE-Sanandaj City): a key for exploration of copper and gold mineralisation. Research Journal of Applied Sciences, 2 (96): 763-768. https://medwelljournals.com/abstract/?doi=rjasci.2007.763.768

Beane, R.E., 1982. Hydrothermal alteration in silicate rocks, southwestern North America, in Titley, S.R., ed., Advances in geology of the porphyry copper deposits: Univ. Arizona Press, Tucson, 117-137.

Belmouhoub, A., 1995. Rapport sur l'évaluation géochimique de la potentialité de quelques manifestations ferrugineuses du massif de M'Sirda (Algérie Nord-Occidentale). Rapport de fin de cycle C.E.S.E.V, Nancy, 46 p.

Belmouhoub, A., 2004. Les minéralisations sulfurées à Cu, (Au), Pb-Zn associées aux roches volcaniques miocènes du massif de Tifferaouine (Sahel oranais): Pétrographie, géochimie et prospection minière. Magister thesis, U.S.T.H.B, Algiers, 130 p.

Benali, H., 2007. Les minéralisations associées aux roches magmatiques tertiaires du Nord de l'Algérie: Typologie, pétrologie, cadre géodynamique et implications métallogéniques. Thèse de doctorat, U. S. T. H. B, Alger, 173 p.

Boardman, J.W., 1998. Leveraging the high dimensionality of AVIRIS data for improved subpixel target unmixing and rejection of false positives: mixture tuned matched filtering. In: Pasadena, CA. Summaries of the Seventh Annual JPL Airborne Geoscience Workshop, 6.

Boardman, J.W., Kruse, F.A., 1994. Automated spectral analysis: a geological example using AVIRIS data, north Grapevine Mountains, Nevada. Tenth Thematic Conference on Geologic Remote Sensing, Environmental Research Institute of Michigan: 1407-1418.

Buenemann, M., Martius, C., Jones, J.W., Herrmann, S.M., Klein, D., Mulligan, M., Reed, M.S., Winslow, M., Washington-Allen, R.A., Lal, R., Ojima, D., 2011. Integrative geospatial approaches for the comprehensive monitoring and assessment of land management sustainability: Rationale, Potentials, and Characteristics. Land degradation and development, 22 (2): 226-239. https://doi.org/10.1002/ldr.1074

Cardoso-Fernandes, J., Teodoro, A., Alexandre, L., 2019. Remote sensing data in lithium (Li) exploration: A new approach for the detection of Li-bearing pegmatites. International Journal of Applied Earth Observation and Geoinformation, 76: 10-25. https://doi.org/10.1016/j.jag.2018.11.001

Cardoso-Fernandes, J., Teodoro, A.C., Lima, A., Menuge, J., Brönner, M., Steiner, R., 2022. Sentinel-1 and ALOS data for lineament extraction: a comparative study. Earth Resources and Environmental Remote Sensing/GIS Applications XIII, Berlin, Germany, 122680X. https://doi.org/10.1117/12.2636117

Ciszak, R., 1993. Evolution géodynamique de la chaîne tellienne en Oranie (Algérie occidentale) pendant le Paléozoique et le Mésozoique. Thèse de doctorat, Univ. Toulouse, 513 p.

Clark, R.N., King, T.V.V., Klejwa, M., Swayze, G.A., Vergo, N., 1990. High spectral resolution reflectance spectroscopy of minerals. Journal of Geophysical Research: Solid Earth, 95: 12653-12680. https://doi.org/10.1029/JB095iB08p12653

Clark, R.N., Swayze, G.A., Gallagher, A., King, T.V.V., Calvin, W.M., 1993. The U.S. Geological Survey, digital spectral library: version 1: 0.2 to 3.0 microns. U.S. Geological Survey Open File Report: 93-592. https://doi.org/10.3133/ofr93592

Cudahy, T., Jones, M., Thomas, M., Laukamp, C., Caccetta, M., Hewson, R., Verrall, M., 2008. Next generation mineral mapping in Queensland: another piece to the precompetitive geoscience data puzzle, Australian Earth Sciences Convention (AESC): 20-24.

Da Cunha Frutuoso, R.M., 2015. Mapping hydrothermal gold mineralization using Landsat 8 data. A case of study in Chaves license, Master thesis, Univ. Porto, Portugal, 85 p.

Ducart, D.F., Silva, A.M., Toledo, C.L.B., Assis, L.M.D., 2016. Mapping iron oxides with Landsat-8/OLI and EO-1/Hyperion imagery from the Serra Norte iron deposits in the Carajás Mineral Province, Brazil. Brazilian Journal of Geology, 46 (3): 331-349. https://doi.org/10.1590/2317-4889201620160023

Eisele, A., Lau, I., Hewson, R., Carter, D., Wheaton, B., Ong, C., Kaufmann, H., 2012. Applicability of the thermal infrared spectral region for the prediction of soil properties across semi-arid agricultural landscapes. Remote Sensing, 4 (11): 3265-3286. https://doi.org/10.3390/rs4113265

Eldosouky, A.M., Abdelkareem, M., Elkhateeb, S.O., 2017. Integration of remote sensing and aeromagnetic data for

mapping structural features and hydrothermal alteration zones in Wadi Allaqi area, South Eastern Desert of Egypt. Journal of African Earth Sciences, 130: 28-37. https://doi.org/10.1016/j.jafrearsci.2017.03.006

ENVI Tutorial., 2013. Exelis visual information solutions. Boulder, Colorado.

Fenet, B., 1975. Recherches sur l'alpinisation de la bordure septentrionale du bouclier africain à partir de l'étude d'un élément de l'orogène nord maghrébin, les monts de Djebel Tessala et les massifs du littoral oranais. Thèse de doctorat, Univ. Nice, 301 p.

Frutuoso, R., Lima, A., Teodoro, A.C., 2021. Application of remote sensing data in gold exploration: targeting hydrothermal alteration using Landsat 8 imagery in northern Portugal. Arabian Journal of Geosciences, 14: 1-18. https://doi.org/10.1007/s12517-021-06786-0

Glaçon, J., 1967. Recherches sur la géologie et les gîtes métallifères du Tell sétifien (Algérie). Publications du Service géologique de l'Algérie, nouvelle série, Bulletin, no. 32.

Goetz, A.F., Rock, F., Hand Rowan, B.N., 1983. Remote sensing for exploration, an overview. Economic Geology, 78: 573-590. https://doi.org/10.2113/gsecongeo.78.4.573

Green, A.A., Berman, M., Switzer, P., Craig, M. D., 1988. A transformation for ordering multispectral data in terms of image quality with implications for noise removal. IEEE Transactions on Geoscience and Remote Sensing, 26 (1): 65-74. https://doi.org/10.1109/36.3001

Guardia, P., 1975. Géodynamique de la marge alpine du continent africain d'après l'étude de l'Oranie Nord Occidentale. Relations structurales et paléogéographiques entre le Rif externe: le Tell et L'avant-pays atlasique. Univ. Nice, 286 p.

Gupta, R.P., 2003. Remote sensing geology. Springer Berlin, Heidelberg, 428 p. https://doi.org/10.1007/978-3-662-05283-9

Gupta, R.P., 2017. Remote sensing geology. Springer. https://doi.org/10.1007/978-3-662-55876-8

Harsanyi, J.C., Chang, C.I., 1994. Hyperspectral image classification and dimensionality reduction: An orthogonal subspace projection approach. IEEE Transactions on Geoscience and Remote Sensing, 32: 779-785. https://doi.org/10.1109/36.298007

Himri, Y., Boudghene Stambouli, A., Draoui, B., Himri, S., 2008. An investigation on wind power potential in Tindouf region Algeria. Proceedings of world academy of science, engineering and technology, 33 (7): 1128-1136. https://doi.org/10.1016/j.rser.2008.09.007 http://earthexplorer.usgs.gov [Consulted on 17 March 2014]. https://landsat.gsfc.nasa.gov [Consulted on 10/06/2014].

Hu, B., Xu, Y., Wan, B., Wu, X., Yi., G., 2018. Hydrothermally altered mineral mapping using synthetic application of Sentinel-2A MSI, ASTER and Hyperion data in the Duolong area, Tibetan Plateau, China. Ore Geology Reviews, 101: 384-397. https://doi.org/10.1016/j.oregeorev.2018.07.017

Hunt, G.R., 1977. Spectral signatures of particulate minerals in the visible and near infrared, Geophysics, 42: 501-513. https://doi.org/10.1190/1.1440721

Ibrahima, E., Barnabéa, P., Ramanaidoub, E., Pirarda, E., 2018. Mapping mineral chemistry of a lateritic outcrop in new Caledonia through generalized regression using Sentinel-2 andfield reflectance spectra. International Journal of Applied Earth Observation and Geoinformation, 73: 653-665. https://doi.org/10.1016/j.jag.2018.08.004

Inzana, J., Kusky, T., Higgs, G., Tucker, R., 2003. Supervised classifications of Landsat TM band ratio images and Landsat TM band ratio image with radar for geological interpretations of central Madagascar. Journal of African Earth Sciences, 37: 59-72. https://doi.org/10.1016/S0899-5362(03)00071-X

Jensen, J.R., 1996. Introducing digital image processing: A remote sensing perspective; 2nd, Prentice Hall Series in geographic information Siences. l'Université du Michigan, 318 p.

Jensen, J.R., 2005. Introductory Digital Image Processing: A Remote Sensing Perspective. 3rd Edition, Prentice Hall, Upper Saddle River. l'Université de Californie, 526 p.

Megartsi, M., 1985. Le volcanisme Mio-Plio-quaternaire de l'Oranie nord occidentale, 296 p.

Mia, B., Fujimitsu, Y., 2012. Mapping hydrothermal altered mineral deposits using Landsat 7 ETM+ image in and around Kuju volcano, Kyushu, Japan. Journal of Earth System Science, 121 (4): 1049- 1057. https://doi.org/10.1007/s12040-012-0211-9

Mina, Z., Peyman, A., Reza, N., 2019. Determination of Hydrothermal Alteration Zones Using Remote Sensing Methodes in Tirka Area, Toroud, NE Iran. Journal of the Indian Society of Remote Sensing, 47: 1817-1830. https://doi.org/10.1007/s12524-019-01032-3

Mouffok, K., Boukhechba, M., 1999. Contibution à l'étude petrographique et gîtologique du massif de Tifferaouine (Sondage TS 15). Mémoire d'ingéniorat d'état, USTHB, 157 p.

Mwaniki, M.W., Moeller, M.S., Schellmann, G., 2015. A comparison of Landsat-8 (OLI) and Landsat-7 (ETM+) in mapping geology and visualising lineaments: a case study of central region Kenya. The International Archives of the Photogrammetry, Remote Sensing and Spatial Information Sciences, 7 (W3): 897-903. https://doi.org/10.5194/isprsarchives-XL-7-W3-897-2015

Nait Amara, B., Aissa, D.E., Maouche, S., Braham, M., Machane, D., Guessoum, N., 2019. Hydrothermal alteration mapping and structural features in the Guelma basin (Northeastern Algeria): contribution of Landsat-8 data. Arabian Journal of Geosciences, 12, 94. https://doi.org/10.1007/s12517-019-4224-4

Ninomiya, Y., 2003. A stabilized vegetation index and several mineralogic indices defined for ASTER VNIR and SWIR data. In Geoscience and Remote Sensing Symposium, 2003. IGARSS'03. Proceedings, 3: 1552-1554.

O'Leary, D.W., Friedman, J.D., Pohn, H.A., 1976. Lineament, Linear, Lineation: Some proposed new standard for old terms. Geological Society of America Bulletin, 87: 1463-1469. https://doi.org/10.1130/0016-7606(1976)87<1463:LLLSPN>2.0.CO;2

Peleli, S., Kouli, M., Marchese, F., Lacava, T., Vallianatos, F., Tramutoli, V., 2021. Monitoring temporal variations in the geothermal activity of Miocene Lesvos volcanic field using remote sensing techniques and MODIS – LST imagery, International Journal of Applied Earth Observation and Geoinformation, 95. https://doi.org/10.1016/j.jag.2020.102251

Pique, A., Brahim, L.A., Ouali, R.A., Amrhar, M., Charroud, M., Gourmelen, C., Tricart, P., 1998. Evolution structurale des domaines atlasiques du Maghreb au Méso-Cénozoïque; le rôle des structures héritées dans la déformation du domaine atlasique de l'Afrique du Nord. Bulletin de la Société Géologique de France, 169 (6): 797-810.

Pontual, S., Merry, N., Gamson, P., 2008. Spectral Analysis Guides for Mineral Exploration. Ausspec International Ltd, Victoria, 189 p.

Pour, A., Hashim, M., 2015. Hydrothermal alteration mapping from Landsat-8 data, Sar Chesmeh copper mining district, south-eastern Islamic Republic of Iran. Journal of Taibah University for Science, 9: 155-166. https://doi.org/10.1016/j.jtusci.2014.11.008

Pour, A.B., Hashim, M., Genderen, J.V., 2013. Detection of hydro- thermal alteration zones in a tropical region using satellite remote sensing data: Bau goldfield, Sarawak, Malaysia, Ore Geology Reviews, 54: 181–196. https://doi.org/10.1016/j.oregeorev.2013.03.010

Rameshchandra, P., 2014. A gis based correlation between lineaments and gold occurences of ramagiri-penakacherlaschist belt, Eastern Dharwar craton, India. International Journal of Geology, Earth and Environmental Sciences, (4): 259-267.

Rockwell, B.W., 2013. Automated mapping of mineral groups and green vegetation from Landsat Thematic Mapper imagery with an example from the San Juan Mountains, Colorado. Scientific Investigations Map, 3252. https://doi.org/10.3133/sim3252

Rowan, L.C., Goetz, A.F.H., Ashley, R.P., 1977. Discrimination of hydrothermally altered and unaltered rocks in visible and near infrared multispectral images. Geophysics, 42 (3): 522-535. https://doi.org/10.1190/1.1440723

Sabins, F.F., 1999. Remote sensing for mineral exploration. Ore Geology Reviews, 14 (3-4): 157-183. https://doi.org/10.1016/S0169-1368(99)00007-4

Santos, D., Cardoso-Fernandes, J., Lima, A., Teodoro, A. C., 2022. The potential of spectral unmixing method applied to PRISMA hyperspectral images in the identification of Li minerals: an evaluation for prospecting purposes. Paper presented at the SPIE Remote Sensing, Earth Resources and Environmental Remote Sensing /GIS Applications XIII, Berlin, Germany. https://doi.org/10.1117/12.2636034

Scheidt, S., Ramsey, M., Lancaster, N., 2008. Radiometric normalization and image mosaic generation of ASTER thermal infrared data: an application to extensive sand and dune fields. Remote Sensing of Environment, 112: 920-933. https://doi.org/10.1016/j.rse.2007.06.020

Schott, J.R., E.B., 2007. Remote Sensing: The Image Chain Approach, second ed. Oxford University Press, New York, 688 p.

Segal, D.B., 1983. Use of Landsat multispectral scanner data for definition of limonitic exposure in heavily vegetated areas, El Raso Texas, Economic Geology, 78 (4): 711-722. https://doi.org/10.2113/gsecongeo.78.4.711

Souhalia, A., 2001. Contribution à l'étude pétrographique et gîtologique du massif de Tifferaouine (Sondage T22). Mémoire d'ingéniorat d'état, USTHB, 87 p.

Torres-Vera, M.A., Prol-Ledesma, R.M., 2003. Spectral enhancement of selected pixels in thematic mapper images of the Guanajuato district (Mexico) to identify hydrothermally altered rocks. International Journal of Remote Sensing, 24 (22): 4357-4373. https://doi.org/10.1080/0143116031000075134

Turner, DJ., Rivard, B., Groat, LA., 2014. Visible and short-wave infrared reflectance spectroscopy of REE phosphate minerals. American Mineralogist, 99: 1335-1346. https://doi.org/10.2138/am.2014.4674

Van der Meer, F.D., Van derWerff, H.M.A., Van Ruitenbeek, F.J.A., Hecker, C.A., Bakker, W.H., Noomen, M.F., Woldai, T., 2012. Multi- and hyperspectral geologic remote sensing: a review. International Journal of Applied Earth Observation and Geoinformation, 14 (1): 112-128. https://doi.org/10.1016/j.jag.2011.08.002

Wang, G., Du, W., Carranza, E.J.M., 2017. Remote sensing and GIS prospectivity mapping for magmatic-hydrothermal base- and precious-metal deposits in the Honghai district, China. Journal of African Earth Sciences, 128: 97-115. https://doi.org/10.1016/J.JAFREARSCI.2016.06.020

Woldai, T., Amera, S.A, Carranza, E.J.M., Jemwa, G., Duke, E.F., 2010. Spectral remote sensing of hydrothermal alteration associated with volcanogenic massive sulphide deposits, Gorob-Hope Area, Namibia. 8th International AARSE Conference, Addis Ababa, Ethiopia, 25-29.

Yousefi, M., Tabatabaei, S.H., Rikhtehgaran, R., Pour, A.B., Pradhan, B., 2021. Application of Dirichlet Process and Support Vector Machine Techniques for Mapping Alteration Zones Associated with Porphyry Copper Deposit Using ASTER Remote Sensing Imagery. Minerals, 11 (11): 1-25. https://doi.org/10.3390/min11111235

Zanter, K., 2016. Landsat 8 (L8) Data Users Handbook. Department of the Interior U.S. Geological Survey, South Dakota, 106 p.

MANUSCRITO RECIBIDO: 2-9-2022
REVISIÓN RECIBIDA: 26-4-2023
ACEPTACIÓN DEL MANUSCRITO REVISADO: 25-5-2023